Imaging-Based Methods for Non-invasive Assessment of Bone Properties Influenced by Mechanical Loading

Norma J. MacIntyre, BSc(PT), MSc, PhD; Amanda L. Lorbergs, BSc, MSc

ABSTRACT

Purpose: To describe the most common in vivo imaging-based research tools used to assess bone properties that are influenced by mechanical loading associated with exercise, habitual physical activity, or disease states. Bone is a complex metabolically active tissue that adapts to changes in mechanical loading by altering the amount and spatial organization of mineral. *Method:* Using a narrative review design, the authors provide an overview of bone biology and biomechanics to emphasize the importance of bone size scale, porosity, and degree of mineralization when interpreting measures acquired using quantitative ultrasound (QUS), dual-energy X-ray absorptiometry (DXA), computed tomography (CT), magnetic resonance imaging (MRI), and finite element analysis (FEA). For each imaging modality, basic imaging principles, typical outcome measures associated with changes in mechanical loading, and salient features for physiotherapists are described. *Main Results:* While each imaging modality has strengths and limitations, currently CT-based methods are best suited for determining the effects of mechanical loading on bone properties—particularly in the peripheral skeleton. *Conclusions:* Regardless of the imaging technology used, the physiotherapist must carefully consider the assumptions of the imaging-based method, the clinical context, the nature of the change in mechanical loading, and the expected time course for change in bone properties.

Key Words: adult; bone and bones; weight-bearing; diagnostic imaging; adaptation, physiological.

RÉSUMÉ

Objectif : Décrire les outils de recherche en imagerie *in vivo* les plus couramment utilisés pour l'évaluation des propriétés des os qui sont influencés par la charge mécanique associée à l'exercice, à l'activité physique habituelle ou aux problèmes de santé. Les os sont des tissus actifs complexes sur le plan métabolique, qui s'adaptent aux changements de la charge mécanique en modifiant la quantité et l'organisation spatiale des minéraux. *Méthode :* À l'aide d'un modèle de revue narrative, un aperçu de la biologie et de la biomécanique osseuse est produit en vue de mettre l'accent sur l'importance de l'échelle de la dimension des os, de la porosité et du degré de minéralisation au moment d'interpréter les mesures recueillies à l'aide d'ultrasons quantitatifs (QUS), d'absorptiométrie à rayons X biphotonique (DXA), de tomographie informatisée (CT), d'imagerie par résonance magnétique (IRM) et d'analyse par éléments finis (FEA). Pour chaque modalité d'imagerie, les principes d'imagerie de base, les mesures typiques de résultats associés aux changements de charge mécanique et les caractéristiques principales pour les physiothérapeutes ont été décrits. *Principaux résultats :* Bien que chaque modalité d'imagerie ait ses forces et ses limites, les méthodes à base de tomographie informatisée sont les mieux adaptées pour déterminer les effets de la charge mécanique sur les propriétés osseuses – particulièrement dans le squelette périphérique. *Conclusions :* Sans égard à la technologie d'imagerie utilisée, le physiothérapeute doit analyser soigneusement les hypothèses de la méthode fondée sur l'imagerie, le contexte clinique, la nature du changement de charge mécanique et le délai attendu de changement des propriétés osseuses.

At entry to practice, physiotherapists need to understand the principles of medical imaging to interpret X-rays and radiology reports pertaining to the people on their caseload. Recently, physiotherapy scope of practice in several Canadian provinces has been expanded to include ordering musculoskeletal imaging studies such as ultrasound (US), X-ray, and magnetic resonance imaging (MRI). In this clinical context, physiotherapists must understand the indications and diagnostic utility of different imaging procedures used for routine clinical investigations to incorporate these tools into practice. With respect to bone health in adulthood, diagnostic imaging is used to identify osteoporosis and the risk or presence of fracture. However, diagnostic imaging of bone is beyond

Size Scale

cm

μm

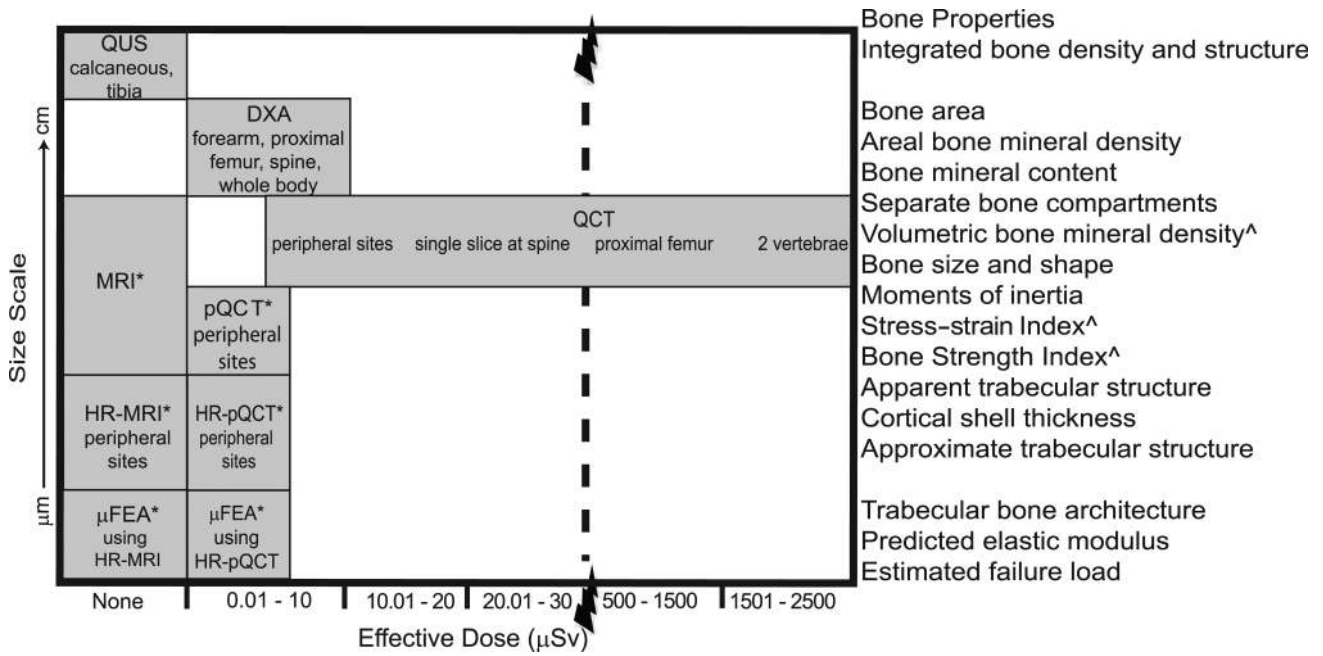| QUS calcaneous, tibia | | | | | | Bone Properties Integrated bone density and structure |
	DXA forearm, proximal femur, spine, whole body					Bone area Areal bone mineral density Bone mineral content
MRI*		QCT peripheral sites single slice at spine proximal femur 2 vertebrae				Separate bone compartments Volumetric bone mineral density^ Bone size and shape
	pQCT* peripheral sites					Moments of inertia Stress–strain Index^ Bone Strength Index^
HR-MRI* peripheral sites	HR-pQCT* peripheral sites					Apparent trabecular structure Cortical shell thickness Approximate trabecular structure
μFEA* using HR-MRI	μFEA* using HR-pQCT					Trabecular bone architecture Predicted elastic modulus Estimated failure load
None	0.01 – 10	10.01 – 20	20.01 – 30	500 – 1500	1501 – 2500	

Effective Dose (μSv)

Figure 1   Bone size scale (μm to cm) capable of being imaged by each modality and the corresponding bone properties shown as a function of the effective radiation dose (μSv).
*Primarily used for research rather than clinical purposes.
^Not measured by MRI.
QUS = quantitative ultrasound; DXA = dual-energy X-ray absorptiometry; MRI = magnetic resonance imaging; QCT = quantitative computed tomography; pQCT = peripheral QCT; HR = high resolution; μFEA = micro finite element analysis.

the scope of this review. (Readers interested in diagnostic imaging related to bone health are referred to several reviews describing advances in bone-imaging techniques for diagnosing osteoporosis, classifying fracture risk, and assessing fracture healing.[1–3]) The current review focuses on in vivo imaging methods and novel research tools developed to assess changes in bone properties in the adult skeleton that may be influenced by mechanical loading. Several recent reviews have described the effects of increased mechanical loading (exercise, functional electrical stimulation, etc.) on bone properties in individuals during normal ageing or with injuries or disease states associated with reduced mechanical loading and/or accelerated bone loss (primary osteoporosis, spinal-cord injury, stroke, cancer, etc.).[4–8] For example, a systematic review of trials using peripheral quantitative computed tomography (pQCT) to evaluate the effect of exercise and physical activity on bone in postmenopausal women concluded that high loads, novel loading directions, and/or direct loads on bone have modest, site-specific benefits— particularly noted in cortical bone.[6] The current review describes the imaging-based measures used in these trials and some emerging methods that may be incorporated in future clinical trials. It is important to note that the precision of these in vivo measures varies from 2% to 5% and that few studies to date are of sufficient duration (at least 2 years) to determine the effect of increased mechanical loading on bone when the rate of change

is relatively slow (i.e., with ageing[4–6] or cancer[7]). While adaptations to mechanical loading may be observed within 6 to 12 months among individuals with injuries or disease states associated with accelerated bone loss (e.g., in the knee region following spinal-cord injury),[8] the long-term benefits of increased mechanical loading in these individuals are not clear. Properties of bone can be measured— at different scales—using tools based on US, dual-energy X-ray absorptiometry (DXA), computed tomography (CT), and MRI. Figure 1 illustrates the resolution and associated scale of the bone properties as a function of the radiation exposure associated with each method reviewed. For each imaging modality, we discuss the imaging principles, examples of bone properties linked with changes in mechanical loading that can be estimated, and the salient features for physiotherapists to consider.

BACKGROUND

Bone tissue has a mechanical sensing apparatus that adjusts bone properties in response to the forces imposed on the skeleton. That is, bone remodels to meet the functional needs of the body and has the capacity for repair. Muscle activity produces the mechanical forces experienced by the skeleton, which are critical to the maintenance of bone health in adulthood.[9] Several bone properties contribute to whole-bone strength; bone density, size, shape or distribution of the mineral, rate of turnover, damage accumulation, and extent of mineral-

ization are important determinants.[10] Medical-imaging-based research methods enable the quantification of anatomic features of bone at various resolutions and scales to estimate skeletal adaptations to altered mechanical loading in vivo.

Bone composition

The skeleton serves several important mechanical and metabolic functions. Mechanically, bones protect vital organs from injury, amplify sound waves, and provide a stable framework that enables muscle contractions to generate force and movement. Metabolically, the skeleton provides mineral storage capacity (99% of calcium and 85% of phosphorus in the body are stored in the bones) and traps toxic minerals such as lead. Bone tissue is composed of organic and inorganic materials, which makes it well suited to perform these functions. The organic component (primarily collagen) provides a compliant matrix that balances the brittle inorganic component (primarily hydroxyapatite, an insoluble salt of calcium and phosphorus) to better resist fracture. Although many factors must be considered when bone fails to meet metabolic demands, failure to meet mechanical demands is typically indicated by fracture. Simply put, a bone breaks when the loads applied to it exceed its strength. (In this review *strength* is defined as the competence of the whole bone to absorb energy, dissipate it, and repair the fatigued material, unless otherwise noted.) The balance between organic and inorganic materials differs according to the skeletal site, metabolic demands, and primary mechanical function(s) of the bone.

Ongoing repair, mobilization of mineral stores, and adaptive (re)shaping of the skeleton occur through bone turnover. In adults, bone turnover primarily involves a process called "remodelling," which is tightly coupled in time and space to repair fatigued bone that is unable to withstand typical loads and to adapt the bone in response to altered metabolic demands or mechanical loads.[11] The rate of bone turnover is determined by the number of remodelling units within a given space. This process of remodelling in response to mechanical stimuli is summarized briefly below; for a detailed animated review see the American Society for Bone and Mineral Research Web site.[12]

Bone turnover is triggered by microcracks that form to dissipate absorbed energy and by significant variations in the rate of fluid flow through the bone matrix (modulated by mechanical loading).[9,11] The major responders are three types of bone cells: osteocytes, osteoclasts, and osteoblasts. The *osteocytes* (cells embedded in the mineralized bone tissue) in proximity to the microcracks or altered shear forces undergo programmed cell death (apoptosis) and stop secreting the protein sclerostin, which normally acts to inhibit bone turnover.[12] The neighbouring osteocytes detect the altered strain and secrete factors that, combined with the lack of sclerostin,

recruit precursor cells from the marrow to form osteoclasts.[12] *Osteoclasts* create a tunnel through cortical bone, or a ditch on the surface of trabecular bone, that is approximately 200 μm in diameter and progresses at an estimated 40 μm/day over the course of 2 to 3 weeks.[11,13] *Osteoblasts* are then recruited to the resorbed cavity to produce proteins that form the organic matrix. Mineralization is delayed by approximately 10 days after the organic matrix is laid down, but it occurs rapidly during the primary phase, so that 50–70% of maximum mineralization is achieved within 3 to 4 months.[12] The secondary phase of mineralization slows exponentially as the radius of the cavity decreases and mineral density of the cavity slowly increases, perhaps taking several years to complete.[13]

It is estimated that 5% of cortical bone and 25% of trabecular bone in the young-adult skeleton is remodelled each year.[14] The rate of turnover increases in direct relationship with the age-related reduction in mechanical loading, and the loss or gain in bone is determined by the relative activity of osteoclasts and osteoblasts.[15–17] The rate of bone turnover has a dramatic effect on bone strength, fracture risk, and the interpretation of measures acquired using medical imaging. For physiotherapists who aim to improve bone strength through exercise, it is important to remember that bone remodelling and the rate of turnover affect almost all determinants of bone strength, from the micro to the macro level.[10]

Bone size scale

Shapes of the various bones in the human skeleton differ considerably, yet we can generally recognize a mammalian vertebra or femur across species quite easily. This consistency in bone shape may suggest that bones are static structures, and, on the scale of centimetres, this assumption holds. However, when we consider bone on the scale of angstroms, microns, and millimetres, as we did in the previous section, we recognize the highly dynamic nature of bone and its capacity for adaptation and repair.

On a macro level, the skeleton is described as having two major types of bone—cortical and trabecular—which have similar tissue compositions but differ in terms of how the bone material is organized and its degree of porosity. These factors contribute to differences in relative density, defined as the ratio of porous bone density to the physiologic density of nonporous bone tissue—approximately 2.0 g/cm^3.[14] *Cortical bone*, also called compact bone, is composed of osteons, cylindrical layers that surround longitudinally oriented Haversian canals (40–50 μm in diameter).[18,19] Porosity of cortical bone ranges from approximately 5% to 30%[14]; thus, its relative density typically varies from 1.8 to 2.0 g/cm^3. In contrast, *trabecular bone*, also called cancellous bone, is organized in longitudinal layers forming plate- and rod-like structures. Porosity of trabecular bone varies from 30% to more than

90%, because of the presence of large pores filled with bone marrow and blood vessels[14]; as a result, the relative density of trabecular bone typically varies from 0.1 to 1.0 g/cm^3. In both types of bone, fluid-filled canaliculi, number of microcracks, and number and size of resorption cavities contribute to the degree of porosity.[14] An important determinant of bone strength, porosity is challenging to measure in vivo because of the size scale of the pores.[10,14] At the macro level, the distinction between highly porous cortical bone and minimally porous trabecular bone becomes ambiguous.

Cortical bone forms a thick shell in the shaft of long bones, a thin shell at the ends of long bones, and a thin envelope around the vertebral bodies. Trabecular bone is found in cuboid bones, vertebral bodies, and flat bones (e.g., the iliac crest) and at the ends of long bones to reinforce the thinning cortical shell. Recall that the accrual and release of mineral from bone during adulthood occurs primarily through remodelling on bone surfaces, as described above. Because trabecular bone is more porous than cortical bone—accounting for 80% of the surface area of the adult skeleton—it is more metabolically active than cortical bone and responds earlier to factors that change the rate of bone turnover.[11,12] For example, women experience rapid bone loss from late perimenopause (after the first missed period) to early menopause (approximately 4 years after the final menstrual flow) because of the increased rate of bone turnover and increased resorption at the cortical and trabecular bone boundary (endosteal surface).[20,21] Thus, the ability to assess trabecular bone in vivo is likely to be particularly helpful in assessing early changes in bone. A barrier to achieving this aim is the size of the trabecular elements in the adult skeleton: trabecular thickness can vary from 100 to 300 μm, and spacing between the elements can vary from 700 to 2,000 μm with healthy ageing.[22] Furthermore, it may be difficult to appreciate the contribution of the cortical bone to whole-bone strength when the shell can be as thin as 0.38 ± 0.24 mm, according to measures of cadaveric femoral necks from older men.[23]

Bone biomechanics and adaptations to mechanical loading

Bone adapts to habitual mechanical stresses by changing its size and shape—adjusting the amount and spatial distribution of the mineral—to minimize strain in a manner that also improves efficiency of the structure.[24] Bones are (re)shaped to equalize the stresses as much as possible, such that elements carrying no stress are removed and those carrying high levels of stress are reinforced.[24] Adding bone tissue in regions with high mechanical stress is a strategic way to improve bone strength while adding minimal bulk and weight. Indeed, the skeleton responds to both increased and decreased mechanical loading by increasing the rate of bone turnover and redistributing mineral to normalize the stresses.[9]
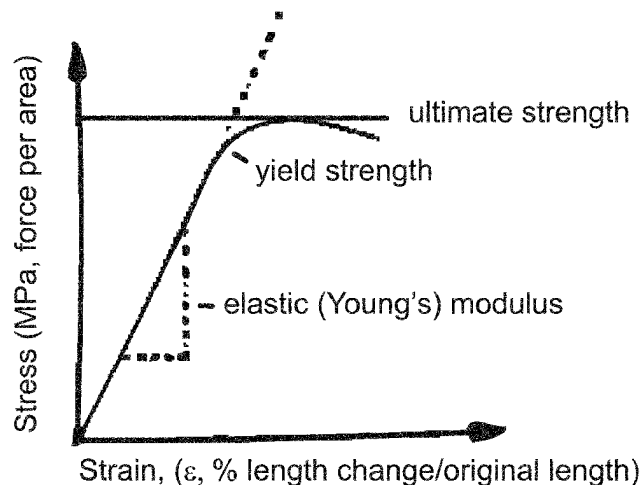

Figure 2   Stress–strain curve for tensile or compressive loading of bone.

Bone specimens have been studied in mechanical testing laboratories to identify the material and geometric properties critical for bone to withstand the loads applied to it. Information about intrinsic bone strength (tissue, not whole) is obtained by using engineering formulae to convert load to stress and deformation to strain to generate a stress–strain curve (see Figure 2).[22] The slope of the stress–strain curve for bone, known as the elastic (or Young's) modulus, provides a measure of the intrinsic stiffness of the bone. The area under the stress–strain curve provides a measure of the amount of energy required to cause material failure (the *modulus of toughness*). The height of the curve is the measure of the ultimate intrinsic material strength of the bone and defines the ultimate strain. Bone-mineral density is highly correlated with material strength and stiffness; the relationship between stiffness and ultimate strain is inverse, however, because highly mineralized bone is brittle.[22] It is important to note that intrinsic bone strength is presented in units of stress and may differ from measures of load or force required to break the bone, since the latter are influenced by several factors extrinsic to the tissue.

Bigger bones absorb more energy before breaking than smaller bones do. Areal bone mineral density (aBMD), measured in g/cm^2, primarily measures the quantity of bone and is a strong predictor of bone strength.[24] In addition, bone geometric properties have established associations with mechanical strength.[24] Interest in evaluating the spatial distribution of bone mineral, rather than aBMD alone, was motivated by the observation that drug therapies for osteoporosis reduced the incidence of fracture by 50% while the corresponding change in aBMD was in the range of 5%.[25] Mechanical testing has demonstrated that a bone's ability to withstand compression and tensile loading is directly proportional to
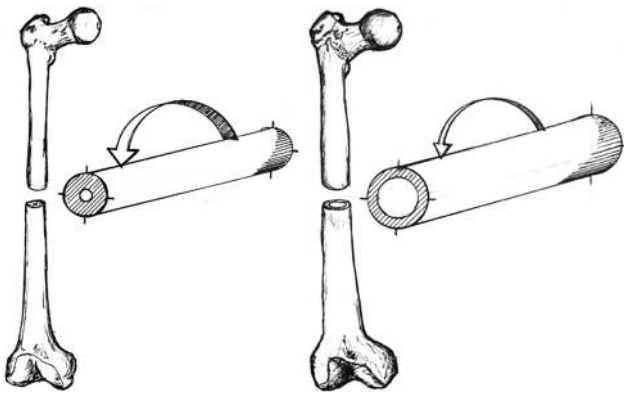
Figure 3 Resistance to bending force in two bone shafts with identical cross-sectional areas, elastic modulus, and stress from axial force but differing in the distance of the material from the centre of the "cylinder." The arrows indicate the magnitude of deformation associated with the same bending force, demonstrating that the shaft on the left cannot resist as much bending force as the one on the right. The midsections of the long bones in the arms and legs gradually become wider and thinner as adults age, becoming more like the bone on the right.

its cross-sectional area (CSA).[22,24] This type of testing has also shown that resistance to bending and torsional loading is proportional to the "second area moment of inertia"—the distance of the mass from the neutral bending axis.[22] The loads typically experienced by the skeleton, particularly the peripheral skeleton, combine compression and tension forces, which generate bending and torsional moments.[24] The skeleton adapts to age-related bone loss by adding bone to the outer (periosteal) surface of long bones and vertebral bodies, thus increasing the bone CSA. This adaptation is more apparent in men; in women, variations are observed based on menopausal status.[26] This adaptive strategy increases the CSA around the neutral axis of bending or torsion (i.e., increases the second area moment of inertia) and preserves strength while requiring a minimal amount of bone mineral (see Figure 3). Increases in mechanical loading preferentially increase mineral accrual on the periosteal bone surfaces in the regions where the mechanical stresses are highest.[24] A recent systematic review concluded that physical activity and/or exercise has a preferential effect on cortical bone size (increased bone-mineral content) and shape (improved spatial distribution of mineral) in postmenopausal women.[5] It is important to note that both of these adaptations are associated with site-specific increases in bone strength.

In the spine, loads on the vertebral bodies are primarily compressive.[24] With ageing, horizontally oriented rod-like trabeculae become thinner and more susceptible to elimination by remodelling activities,[27,28] while vertically oriented plate-like trabeculae are readily perforated by remodelling cavities and become more rod-like in structure.[27] This pattern of loss is detrimental because, for the same decrease in bone mass, loss of tra-

becular connectivity reduces mechanical strength two to five times as much as simple thinning of the trabecular elements,[28] and the plate-like trabeculae may buckle as a result of losing horizontal supports.[29] Several ex vivo studies have shown that the structural arrangement of the trabecular network, not the volume of bone present, determines the mechanical strength of the vertebrae.[30–32] In patients undergoing heart transplantation, changes in the structural arrangement of the trabecular network, not bone-mineral content per unit area, distinguished those with vertebral fracture from those without.[33] Evaluation of trabecular connectivity may provide important information on the ability of the vertebrae to withstand loads—particularly if the forces applied are not of the compressive type that the structure of the trabecular network is designed to resist best.

MEDICAL-IMAGING-BASED METHODS FOR *IN VIVO* ASSESSMENT OF BONE STRENGTH

Bone strength can be estimated using quantitative ultrasound (QUS) and X-ray-based technologies, including DXA and CT (see Figure 1). MRI can be used to estimate apparent trabecular bone structure and, like QUS, involves no exposure to ionizing radiation (see Figure 1), but current methods do not provide estimates of density. Both CT and MRI technologies yield three-dimensional (3D) images and permit the separate assessment of cortical and trabecular compartment bone properties, which is expected to offer distinct advantages for the reasons described above. There are limited options for imaging determinants of bone strength at the structural level in vivo. To date, properties such as spacing and thickness of trabeculae and intra-cortical porosity have been evaluated in bone biopsies taken from the iliac crest and imaged using micro-CT. This approach is invasive, however, and does not permit repeated measurement of the same bone tissue. Post-processing of high-resolution pQCT (HR-pQCT) images and finite element analysis (FEA)–based methods of assessing geometric bone models constructed from whole-body QCT, HR-pQCT, and high-resolution MRI (HR-MRI) are being developed to estimate bone strength at the structural level. These emerging technologies will improve our understanding of the site-specific spatial organization of bone mineral changes in response to altered mechanical loading and its impact on bone strength.

Quantitative ultrasound (QUS)

Measures acquired using QUS relate to bone elasticity, structure of trabeculae, and apparent density.[34] A common measurement site is the non-dominant calcaneus, through which a laterally projecting piezoelectric transducer transmits US energy toward a receiving transducer (which detects the attenuated US signal) on the other side. The velocity and degree of penetration of the sound waves depends on the material they are travel-

ling through.[34] For example, more porous bone allows greater penetration (less attenuation) and lower velocity (slower wave). The calcaneus has several advantages as a QUS measurement site: the bone can be imaged through two nearly plane-parallel surfaces; it consists mainly of trabecular bone, which is more metabolically active than cortical bone; the overlying layer of soft tissue is thin; and it is a weight-bearing bone.[35] QUS devices using a parallel transmitter–receiver probe configuration have been developed to assess transduction of US energy through long bones minimally covered by soft tissue.

Measures of composite bone properties are typically characterized in terms of broadband ultrasound attenuation (BUA, m/s), ultrasound velocity (speed of sound—SOS, dB/MHz), and a calculated stiffness index based on the product of BUA and SOS adjusted by three different constants. Although limited ability to detect change over time in women on drug therapy for osteoporosis has prevented widespread use of QUS,[1] calcaneal BUA did appear to increase in postmenopausal women following 6 months of either weight-bearing or aquatic exercise.[36] In young submariners who experienced limited physical activity (as well as relatively high levels of CO_2, limited exposure to sunlight for vitamin D metabolism, and other changes in lifestyle factors linked with bone health), mid-tibia SOS was decreased after being submerged for 30 days and returned to baseline levels 6 months after returning to shore.[37] Similarly, the stiffness index was significantly lower in the non-affected calcaneus of institutionalized postmenopausal women who had suffered a single-hemispheric stroke more than 6 months previously than in the right calcaneus of healthy age- and gender-matched community-dwelling postmenopausal women.[17]

Commercially available QUS devices are small, portable, and relatively inexpensive and require minimal operator training. Moreover, QUS is non-invasive and can be performed quickly and without exposure to ionizing radiation (see Figure 1). There is emerging evidence that outcomes obtained using QUS are responsive to changes in mechanical loading. However, the integral assessment of bone properties is a major drawback, because it limits our interpretation of the mechanisms contributing to observed changes in BUA, SOS, and/or stiffness index.

Dual-energy X-ray absorptiometry (DXA)

DXA scans are obtained by projecting two X-ray beams with different energies through the part of the body being measured.[38,39] The person lies on the scanner bed with the body part being measured positioned between the X-ray source (located below) and the detector array (positioned above). Attenuation of the beam depends on the interaction between the X-rays and the tissues within the X-ray beam. With appropriate X-ray energies, and assuming that the object being measured consists of two radiologically distinct materials (e.g., bone mineral and

soft tissue; lean tissue and fat tissue), the mass of mineral and soft tissue within the beam can be measured. From an assessment of the total projected area of the bone under investigation, aBMD is calculated as the ratio of bone mineral content (BMC, or mass of mineral) per unit projected area (g/cm^2). Commercial software enables skeletal assessment of the hip, spine, forearm, and whole body, as illustrated in Figure 4.

The clinical diagnosis of osteoporosis is based on T-scores calculated for aBMD at the hip and lumbar spine, because aBMD measured by DXA provides a good estimate of fracture risk in Caucasian postmenopausal women at the population level.[40] The T-score is reported as the number of standard deviations the measure aBMD is from race- and gender-matched young adults at peak aBMD. A T-score ≤ -2.5 falls into the category of osteoporosis, as defined by the World Health Organization based on aBMD in white women.[10] In Canada, the 10-year absolute fracture risk for a particular individual is estimated based on the lowest T-score (hip or lumbar spine) in combination with clinical risk factors.[41] Decreased aBMD has been observed in older adults as a consequence of ageing[40] and following hemiplegic stroke.[42] It is worth noting that aBMD is influenced by changes in bone size.[43] For example, in the presence of a compression fracture in a lumbar vertebra (a hallmark of a weak bone), BMC will not be changed, but the smaller bone area will produce an apparent increase in aBMD. Furthermore, site-specific change in spatial distribution of mineral is not estimated by aBMD.

Bone geometry in terms of area (cm^2) can be extracted for regions of interest within DXA scans (Figure 4A–D). Methods have been developed to extract information about bone shape (spatial distribution of bone mass) at the hip and spine, providing insight into the strength of the whole bone. Hip structural analysis (HSA) software uses the X-ray attenuation profile from the standard two-dimensional (2D) DXA scan of the proximal femur to estimate geometric properties.[44,45] Since 2007, HSA algorithms have been incorporated into the analysis software accompanying DXA scanners manufactured by Hologic Inc. (Bedford, MA). Proximal hip properties such as total surface area of bone, section modulus, cross-sectional (area) moment of inertia, cortical shell thickness, neck shaft angle, and sub-periosteal width can be estimated.[46] Face validity is provided by several large prospective studies reporting that measures of femoral bone geometry derived using this method are predictive of hip fracture.[47,48] However, femoral aBMD and structural properties derived using HSA are very highly correlated, as these measures are based on the same attenuation profile, and thus their independent contributions to risk of hip fracture cannot be distinguished.[49] Clinically pertinent information about shape and size of vertebrae can be obtained from vertebral fracture assessment scans
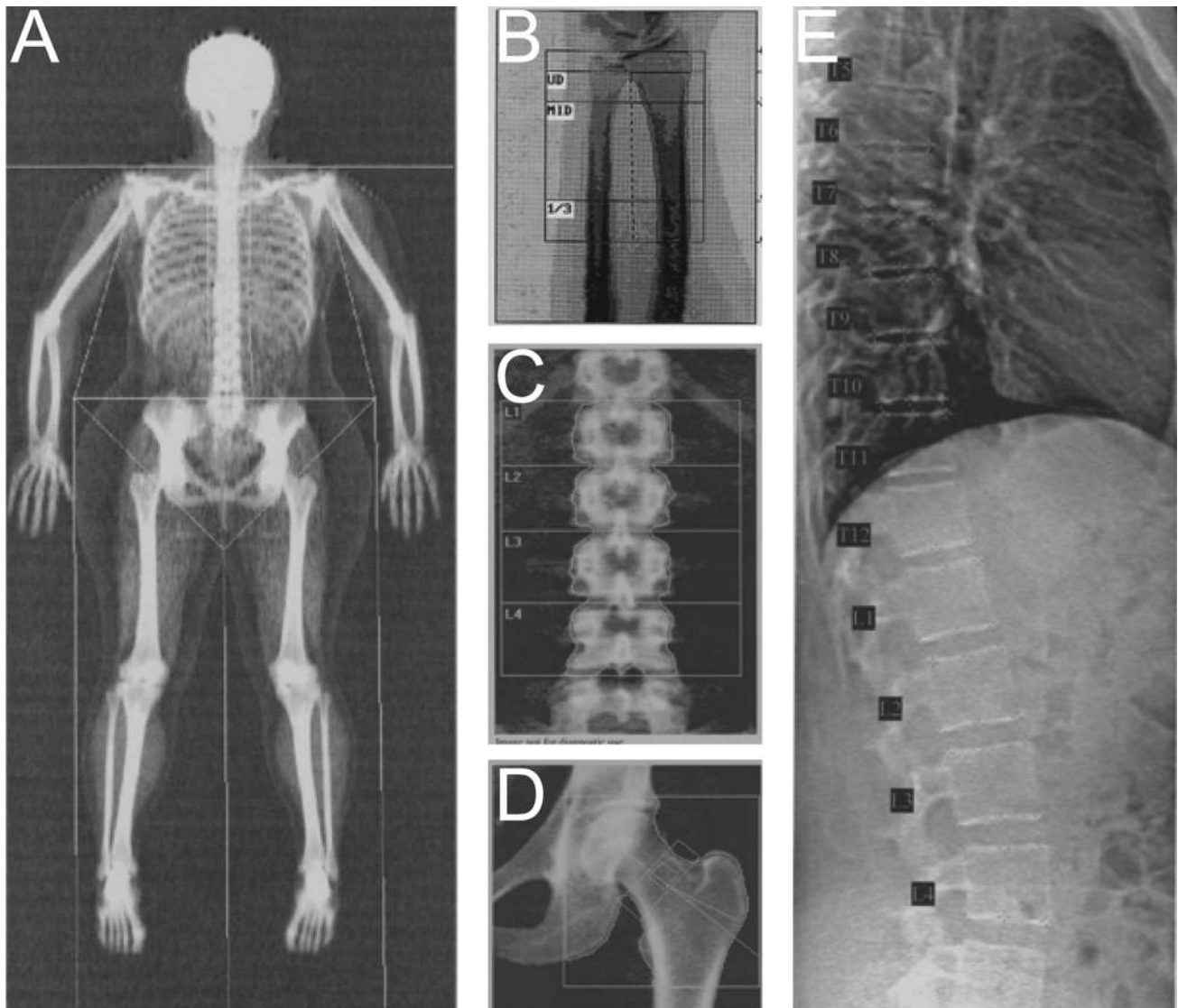
Figure 4 Sample DXA images. Bone density, mass, and area are calculated for each region of interest (defined by semi-automatic line placement) and the total region of interest in scans of the whole body (A), distal forearm (B), lumbar spine (C), and proximal femur (D). Measures of vertebral heights and type and severity of vertebral deformity are derived from semi-automated marker placement on Vertebral Fracture Assessment images of L4 to T4 (E). (All images were acquired using the Hologic Discovery A scanner, except the forearm scan, which was acquired using the Hologic QDR 4500A.)

combined with semi-automatic measures of vertebral body heights. This DXA-based method was used to detect a slower rate of decline in vertebral heights in postmenopausal women with severe osteoporosis of the spine who completed a 12-month home exercise programme relative to the rate in non-exercisers.[50]

DXA is an important clinical tool because of its availability and low levels of radiation exposure, but it is poorly suited to assessing bone adaptations to mechanical loading because of the limitations of projected 2D technology. Moreover, as with any X-ray-based technology, the measured outcomes reflect the amount of mineralized bone. The rate of bone turnover has a direct relationship with the magnitude of increase or decrease in mechanical loading.[51] Over the long term, changes in bone turnover will result in corresponding changes in aBMD, but the initial resorption of mineralized tissue within each remodelling site and the lag time required for remineralization may produce an early decrease in aBMD. It must be noted that aBMD is falsely high in the presence of degenerative joint changes and/or calcification within the vasculature in addition to compression fractures.[43] Finally, it is unclear whether the DXA-based measures of femoral and vertebral bone geometry provide important information in addition to aBMD with respect to bone adaptations to mechanical loading.

Computed tomography (CT)

CT-based methods used to estimate bone properties include whole-body CT, pQCT, and HR-pQCT. Whole-
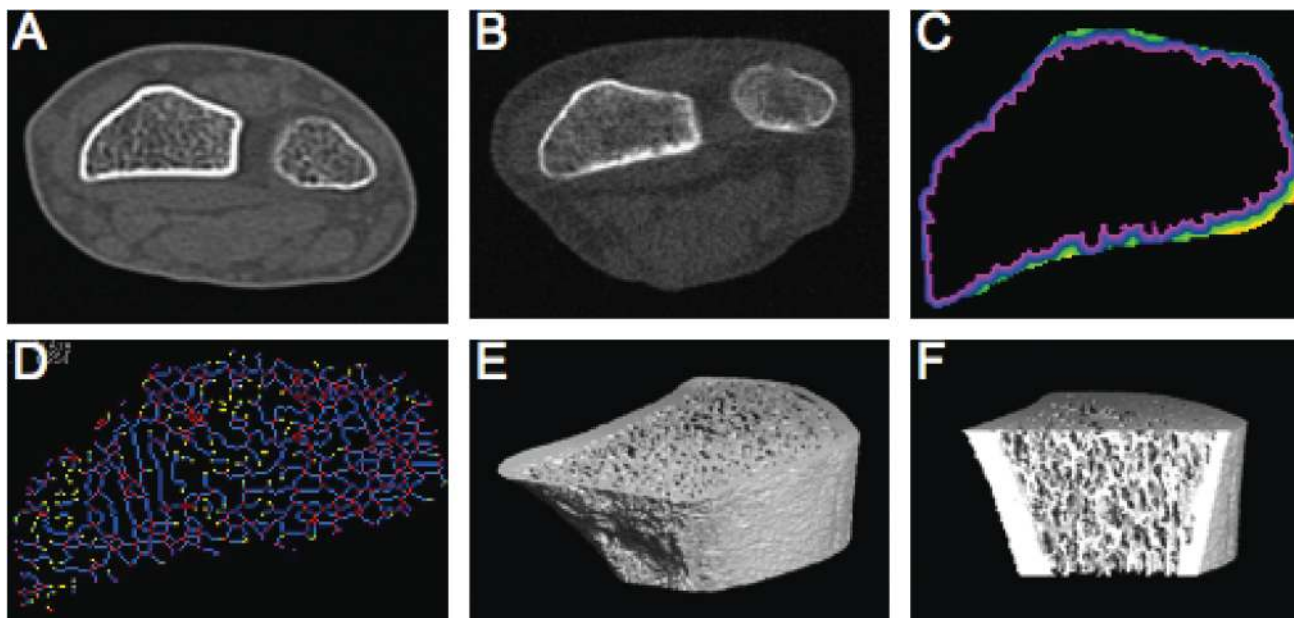
Figure 5 Examples of distal radius images: Cross-sectional image of radius and ulna using whole-body CT (Aquilion CX, Toshiba) (A); improved resolution using pQCT (XCT 960, Stratec) (B); analysis of (B) using OsteoQ software to facilitate analysis of cortical shell thickness (C) and trabecular connectivity (D); ultradistal radius imaged by HR-pQCT (Xtreme, Scanco) (E); and (E) sectioned for analysis of the trabecular network (F)

body CT scanners with spiral technology enable synchronous rotation of the X-ray source and the 64 or 256 multi-detector row, which quantifies (in Hounsfield units) the attenuation of the photon energy as it passes through the body. The inclusion of hydroxyapatite-equivalent calibration standards in the scan acquired using the whole-body CT permits conversion of Hounsfield units to bone-density measurements (g/cm^3); this is referred to as QCT. Volumetric BMD (vBMD, g/cm^3) can be quantified using commercially available packages (QCT Pro, Mindways Software Inc., Austin, TX; Image Analysis Inc., Columbia, KY) or university-based research tools.[52–54] pQCT is specifically designed for assessment of the peripheral skeleton. In Canada, there is no billing code for pQCT, which is therefore used exclusively for research. The most common pQCT models in use today are the XCT 2000(L), which measure the lower leg and forearm, and the XCT 3000, which has a larger bore and accommodates more proximal sites of the peripheral skeleton (both Stratec Medizintechnik, Germany). The HR-pQCT device, the XtremeCT (Scanco Medical, Switzerland), is specifically designed to image bone properties at the ultradistal radius and ultradistal tibia. The pQCT and HR-pQCT scanners are internally calibrated for automatic conversion of Hounsfield units to vBMD values typical of the long bones in the peripheral skeleton.

Any skeletal site can be imaged using the whole-body CT scanner, whereas the peripheral devices are limited by the diameter of the bore (pQCT: 3000 = 00 mm, 2000(L) = 140 mm; HR-pQCT = 126 mm) and the distance from the distal end of the long bone (pQCT: 3000 = 350 mm, 2000L = 400 mm; HR-pQCT = 150 mm). All CT imaging modalities are capable of measuring cortical and trabecular bone compartment properties separately at each site. Typical measures extracted from pQCT scans include vBMD, BMC, and CSA of the total bone compartment and of cortical and trabecular bone/medullary compartments separately. Several cross-sectional geometric properties can be estimated, including average thickness of the cortical shell, second area moment of inertia, and polar moment of inertia.[55] In addition, variables that combine estimates of bone density and geometry, the strength–strain index and bone strength index, are computed to reflect the bone's ability to resist bending along the neutral axis and to resist compression, respectively.[56,57] These geometric measures can be extracted from whole-body CT images—albeit at lower resolutions, and excluding the measures that combine estimates of vBMD—using commercially available dedicated software (BonAlyse, Oy, Jyvaskyla, Finland; OsteoQ reader service, Dundas, ON). Figure 5C illustrates the use of OsteoQ to estimate geometric properties of the cortical shell at the distal radius. OsteoQ also provides estimates of apparent structure of the trabecular network, such as trabecular thickness, spacing and connectivity (Figure 5D), and pore size (average and maximum). As shown in Figure 1, visualization of smaller-scale bone outcomes is enhanced using HR-pQCT, thanks to its nominal spatial resolution of 82 μm^3. Moreover, because the voxels are cubes rather than rectangular prisms (as in whole-body CT and pQCT), the bone properties remain consistent even when they are examined in planes other than the axial plane in which

they were imaged. Typical bone outcomes generated by the Scanco analysis software module include cortical shell thickness, ratio of trabecular bone volume to total tissue volume (trabecular bone volume fraction), trabecular thickness, trabecular spacing, and trabecular number. Custom post-processing software has been developed to quantify cortical thickness and porosity from HR-pQCT images.[58]

In a 12-month trial that used QCT to image the proximal and mid-femur and the tibia in late perimenopausal women randomly assigned to one of four groups—hormone-replacement therapy (HRT), exercises (primarily a progressive high-impact strengthening programme), HRT and exercise, or usual physical activity (control)—an increase in BMC was observed in all three treatment groups.[59] Despite poor adherence in the exercise group, a positive effect was observed in the posterior aspect of the proximal tibia.[59] The combination of HRT and exercise produced the greatest positive adaptations at almost every site measured, since the spatial distribution of mineral was increased in the anterior–posterior regions in those taking HRT only and in both the anterior–lateral and posterior–medial regions in those exercising.[59] The small but significant spatial redistribution of mineral may be very important, given that the bone is strengthened in the weakest direction for resisting bending. In a study using pQCT to image the radii of individuals with residual weakness more than 1 year following a stroke, a reduction in vBMD and BMC was observed in the paretic limb at the distal radius (4% the length of the ulna, where trabecular bone is abundant) and in the cortical bone compartment at the distal third of the radius relative to the non-paretic limb.[60,61] In the paretic lower limb of individuals with chronic stroke, mineral content in the trabecular compartment increased in those who completed a 19-week progressive resistance exercise programme.[62]

The anticipated age-related decreases in femoral-neck CSA, cortical shell thickness, cross-sectional moment of inertia, and section modulus were observed over a 2-year period in postmenopausal women assessed using QCT.[63] Measures of cortical shell thickness derived using pQCT are inversely related to prevalent fracture,[64] reduced with disuse due to stroke,[60,61] and responsive to a 19-week exercise programme in the paretic lower limb of individuals with chronic stroke.[62] In a group of older adults with hemiplegia due to chronic stroke, the strength–strain index at the tibial shaft was associated with muscle quality.[65] These data demonstrate the advantage of assessing geometric properties for the cortical and trabecular compartments separately to characterize adaptations to altered mechanical loading.

The measures of bone geometry described above cannot describe the critical contribution of spatial distribution of bone in the trabecular network. Because of the limited resolution of whole-body CT and pQCT (see Figure 1)

and the size of the trabecular elements (trabecular thickness: 100–300 μm; trabecular spacing: 700–2,000 μm),[11,22] the true architecture of the trabecular network cannot be measured using CT and pQCT. However, the measures of apparent structure demonstrate face validity. Gordon and colleagues (1998) quantified the apparent trabecular structure of the spine using whole-body CT and found that the average marrow pore size (representing trabecular spacing) distinguished women with fractures from those without.[66] Estimates of average marrow pore size at the distal radius, derived from pQCT images (XCT960, Stratec) with an in-plane resolution of 0.3 mm^2 and a slice thickness of 2.5 mm, also distinguished women with wrist fractures from those with no fractures after controlling for vBMD.[67] Using the same measures of apparent trabecular bone structure to investigate side-to-side differences at the distal radius, another study found that average marrow pore size was larger and trabecular connectivity was poorer in the radius of the non-dominant arm than in the dominant one.[68] Using an earlier HR-pQCT model manufactured by Scanco, with an in-plane resolution of 0.35 mm^2 (at the radius) to 0.45 mm^2 (at the tibia) and a slice thickness of 1.5 mm, Riggs and colleagues observed the expected age- and sex-related differences in apparent bone structure in the Minnesota population.[69] Using the latest model of the HR-pQCT, the Xtreme, the same investigators were able to show that the rate of bone-volume loss is the same for men and women, but the pattern of loss differs[70]: women have increased trabecular spacing and decreased trabecular number with age, while men have slow trabecular thinning with little net change in trabecular spacing and trabecular number.[70] To date, research using HR-pQCT has focused on estimating fracture risk.[71–73] Studies are needed to determine whether these measures detect change resulting from altered mechanical loading.

Observing compartmental bone tissue adaptations that result from mechanical (un)loading is an important advantage of imaging with CT technology. Nonetheless, CT image acquisition and assessment are not without limitations. Image acquisition using CT may be limited by factors such as high equipment costs, required operator training, physical dimensions of the device, image resolution, or effective radiation dose. Improved resolution minimizes the error attributable to the partial-volume effect (when a voxel represents more than one tissue type), but the trade-off for increased resolution is increased radiation exposure (see Figure 1). Promising methods of image post-processing have been developed to minimize the impact of partial volume and noise artefacts.[74] At present, and in the foreseeable future, CT is the method of choice for determining the effects of mechanical loading on bone properties, particularly in the examination of peripheral skeletal sites.

Magnetic resonance imaging (MRI)

Magnetic resonance imaging uses a strong magnetic field and a sequence of radiofrequency pulses to encode the spatial frequency of protons within the gradient fields to produce 3D images. Hydrogen is the component most frequently studied when MRI is used to image bone. Bone tissue has very low water content, and the protons have a very short T2 relaxation time (an MRI measure reflecting the chemical environment of protons), which means that bone gives no signal in standard MRI and there is no way to estimate bone density. However, water and fat content in the marrow spaces within the trabecular network provide a strong signal, so that T2-dependent MRI can provide indirect images of the trabecular bone in vivo.[75] High-resolution MRI (HR-MRI) is typically performed using surface coils at peripheral sites such as the heel, knee, and wrist to minimize the signal-to-noise ratio, and in vivo methods to quantify the apparent structure of the proximal femur have been developed.[76]

Nikander and colleagues compared MRI-based measures of femoral-neck geometry in athlete populations exposed to different types of loading impacts.[77,78] Athletes in groups classified as odd-impact loading (e.g., soccer and squash) and high-impact loading (e.g., triple jump and high jump) demonstrated 15% and 30% greater cortical area, respectively, relative to the reference group.[78] Resolution approximating that achieved in vivo ($156 \times 156 \times 300\ \mu m^3$) is in the order of trabecular thickness, but partial-volume effects confound measures such that bone-volume fraction and trabecular thickness are overestimated.[79,80] Nevertheless, in vivo measures of apparent trabecular bone structure using HR-MRI in the radius have detected changes associated with ageing, aBMD, and osteoporosis.[81,82] To date, longitudinal studies of adaptations in bone geometry and apparent structure of the trabecular network in response to altered mechanical loading have not used MRI.

The potential of MRI for evaluation of bone properties lies in its ability to depict fine bone detail without exposure to ionizing radiation. At present, in vivo MRI methods do not permit assessment of bone mineral; however, new methods are under development for evaluating the properties of inorganic and organic bone matrix.[83] The major limitations of this novel imaging method are the lack of access to MRI scanners and the necessary coils as well as the time required for imaging and subsequent analyses.

Finite element analysis (FEA) and micro-FEA (µFEA)

Research tools are being developed to construct computer-based 3D geometric models of bone derived from serial transaxial whole-body QCT, HR-pQCT, and HR-MRI imaging using FEA.[84–88] Whole-body QCT images are post-processed using commercially available software to generate $1\ mm^3$ to $3\ mm^3$ bone voxels, which are converted into equally sized "finite elements"—each assigned homogeneous material elastic properties representative of human cortical or trabecular bone, as appropriate. Similarly, µFEA models can be constructed from HR-pQCT and HR-MRI scans of peripheral skeletal sites at even higher nominal resolution to provide a detailed representation of the microstructure. For example, µFEA models constructed according to the method developed by Vilayphiou and colleagues, using software available from Scanco, contain approximately 2 million elements at the radius and 5 million elements at the tibia.[88] "Virtual" loads (i.e., to simulate forces associated with compression, bending, single-leg stance, or sideways fall) are applied to a volumetric region of interest to predict material properties such as elastic modulus, stresses, failure load, and percentage of load carried by different bone sites.[84,85,88–90]

A study using QCT-derived FEA of thoracic and lumbar vertebrae noted gender differences in age-related changes in vertebral body strength.[84] For both men and women, age was positively associated with the proportion of the load carried by the peripheral compartment of the vertebra and negatively associated with the predicted strength of the trabecular compartment.[84] In women, the age-related decrease in vertebral strength was twofold greater than in men, and there was a significant age-related decrease in strength of the peripheral compartment.[84] FEA of QCT images of the proximal femur was conducted for cases ($n = 77$ with hip fracture at follow-up) and sex- and age-matched controls ($n = 249$ with no fracture at follow-up) selected from a population study of 5,500 men and women.[85] After adjustment for total hip aBMD, FEA-computed strength of the femoral head under virtual "fall loading" conditions predicted incident hip fracture in men only.[85] Using HR-pQCT-based µFEA models of the radius and tibia, Vilayphiou and colleagues observed region-specific differences in load distribution between trabecular and cortical bone in a prospective cohort of 1,189 men with and without fractures.[88] At proximal regions, cortical bone sustained more load (72–82%) than trabecular bone; at distal regions, slightly more load (53–58%) was sustained by trabecular bone.[88] In this same cohort of men, measures of microarchitecture and biomechanical properties derived from µFEA of HR-pQCT-based models of the radius and tibia were associated with all types of fractures.[88] "Virtual bone biopsies" for six women taking an anabolic drug treatment of osteoporosis have been generated from HR-MRI images (with a voxel size of $137 \times 137 \times 410\ \mu m^3$) to produce 3D-rendered "cores" having a volume resolution of $23 \times 23 \times 68\ \mu m^3$.[91] Although the sample size was too small for the researchers to draw definitive conclusions, the bone cores for four of the six women demonstrated changes in trabecular architecture[91] consistent with the osteogenic response associated with increased mechanical loading.

It remains unknown whether the structural level bone outcomes derived using these imaging-based technologies will reflect adaptations to altered mechanical loading. However, it is anticipated that these analyses will contribute new knowledge when the method is applied to monitor individual changes in bone microarchitecture and structural properties in response to targeted loading interventions. At this time, apart from the software modules available for QCT and HR-pQCT, the use of this imaging-based method is limited to the developers of this tool, pending further validation.

CONCLUSIONS

Bone is a complex metabolically active tissue that responds to changes in mechanical loading by altering the amount and spatial organization of mineral. A variety of imaging-based research tools are available to estimate changes in bone properties in response to altered mechanical loading. QUS provides estimates of bone quality in the peripheral skeleton without exposure to ionizing radiation. CT-based technologies that reconstruct 3D images are best suited to measure adaptations in mineral distribution but are restricted to peripheral skeletal sites because of the trade-off between resolution and radiation exposure. MRI provides 3D images that can be analyzed to quantify apparent trabecular bone structure in the peripheral skeleton. Further research using FEA tools may demonstrate local changes in bone microarchitecture and structural properties in response to targeted loading interventions.

KEY MESSAGES

Several medical-imaging-based research tools are capable of measuring bone properties to provide insight into bone adaptations to exercise and other factors that alter mechanical loading of the skeleton. Regardless of the imaging technology used, the rate of bone turnover and the extent of tissue mineralization influence the measures obtained. When interpreting research studies reporting imaging-based estimates of bone properties, physiotherapists must also consider the resolution of the imaging tool; the impact of age, metabolic status, and disease process upon which any changes in mechanical loading are imposed; and the length of time between the onset of altered loading and assessment.

REFERENCES

1. Kazakia GJ, Majumdar S. New imaging technologies in the diagnosis of osteoporosis. Rev Endocr Metab Disord. 2006;7(1-2):67–74. http://dx.doi.org/10.1007/s11154-006-9004-2. Medline:17043763
2. Bouxsein ML. Technology insight: noninvasive assessment of bone strength in osteoporosis. Nat Clin Pract Rheumatol. 2008;4(6):310–8. http://dx.doi.org/10.1038/ncprheum0798. Medline:18431371
3. Kalpakcioglu BB, Morshed S, Engelke K, et al. Advanced imaging of bone macrostructure and microstructure in bone fragility and fracture repair. J Bone Joint Surg Am. 2008;90(Suppl 1):68–78. http://dx.doi.org/10.2106/JBJS.G.01506. Medline:18292360
4. Nikander R, Sievänen H, Heinonen A, et al. Targeted exercise against osteoporosis: A systematic review and meta-analysis for optimising

5. Karinkanta S, Piirtola M, Sievänen H, et al. Physical therapy approaches to reduce fall and fracture risk among older adults. Nat Rev Endocrinol. 2010;6(7):396–407. http://dx.doi.org/10.1038/nrendo.2010.70. Medline:20517287
6. Hamilton CJ, Swan VJ, Jamal SA. The effects of exercise and physical activity participation on bone mass and geometry in postmenopausal women: a systematic review of pQCT studies. Osteoporos Int. 2010;21(1):11–23. http://dx.doi.org/10.1007/s00198-009-0967-1. Medline:19504035
7. Winters-Stone KM, Schwartz A, Nail LM. A review of exercise interventions to improve bone health in adult cancer survivors. J Cancer Surviv. 2010;4(3):187–201. http://dx.doi.org/10.1007/s11764-010-0122-1. Medline:20373041
8. Biering-Sørensen F, Hansen B, Lee BS. Non-pharmacological treatment and prevention of bone loss after spinal cord injury: a systematic review. Spinal Cord. 2009;47(7):508–18. http://dx.doi.org/10.1038/sc.2008.177. Medline:19172152
9. Robling AG. Is bone's response to mechanical signals dominated by muscle forces? Med Sci Sports Exerc. 2009;41(11):2044–9. http://dx.doi.org/10.1249/MSS.0b013e3181a8c702. Medline:19812512
10. National Institutes of Health [NIH] Consensus Development Program. Osteoporosis prevention, diagnosis and therapy. NIH Consens Statement. 2000 [cited 2011 Apr 16];17(1):1–36. Available from: http://consensus.nih.gov/historical.htm.
11. Martin RB, Burr DB, Sharkey NA. Analysis of bone remodeling. In: Martin RB, Burr DB, Sharkey NA, editors. Skeletal tissue mechanics. New York: Springer; 1998. p. 79–125.
12. Ott S. American Society for Bone and Mineral Research bone curriculum: bone remodeling [Internet]. Washington (DC): The Society; 2003–8 [updated 2008 Aug 4; cited 2011 May 31]. Available from: http://depts.washington.edu/bonebio/ASBMRed/growth.html#remodel.
13. Boivin G, Meunier PJ. Changes in bone remodeling rate influence the degree of mineralization of bone. Connect Tissue Res. 2002;43(2-3):535–7. http://dx.doi.org/10.1080/03008200290000934. Medline:12489211
14. Martin RB, Burr DB, Sharkey NA. Skeletal biology. In: Martin RB, Burr DB, Sharkey NA, editors. Skeletal tissue mechanics. New York: Springer; 1998. p. 29–78.
15. Vico L, Chappard D, Alexandre C, et al. Effects of a 120 day period of bed rest on bone mass and bone cell activities in man: attempts at countermeasures. Bone. 1987;2:283–94.
16. Zehnder Y, Lüthi M, Michel D, et al. Long-term changes in bone metabolism, bone mineral density, quantitative ultrasound parameters, and fracture incidence after spinal cord injury: a cross-sectional observational study in 100 paraplegic men. Osteoporos Int. 2004;15(3):180–9. http://dx.doi.org/10.1007/s00198-003-1529-6. Medline:14722626
17. Gaudio A, Pennisi P, Bratengeier C, et al. Increased sclerostin serum levels associated with bone formation and resorption markers in patients with immobilization-induced bone loss. J Clin Endocrinol Metab. 2010;95(5):2248–53. http://dx.doi.org/10.1210/jc.2010-0067. Medline:20305005
18. Cooper DML, Thomas CDL, Clement JG, et al. Age-dependent change in the 3D structure of cortical porosity at the human femoral midshaft. Bone. 2007;40(4):957–65. http://dx.doi.org/10.1016/j.bone.2006.11.011. Medline:17223618
19. Britz HM, Thomas CDL, Clement JG, et al. The relation of femoral osteon geometry to age, sex, height and weight. Bone. 2009;45(1):77–83. http://dx.doi.org/10.1016/j.bone.2009.03.654. Medline:19303955
20. Prior JC. Perimenopause: the complex endocrinology of the menopausal transition. Endocr Rev. 1998;19(4):397–428. http://dx.doi.org/10.1210/er.19.4.397. Medline:9715373
21. Ruff CB, Hayes WC. Sex differences in age-related remodeling of the femur and tibia. J Orthop Res. 1988;6(6):886–96. http://dx.doi.org/10.1002/jor.1100060613. Medline:3171769

bone strength throughout life. BMC Med. 2010;8(1):47. http://dx.doi.org/10.1186/1741-7015-8-47. Medline:20663158

22. Huiskes R, van Rietbergen B. Biomechanics of bone. In: Mow VC, Huiskes R, editors. Basic orthopaedic biomechanics and mechanobiology. 3rd ed. Philadelphia: Lippincott Williams & Wilkins; 2005. p. 123–79.

23. Boyce TM, Bloebaum RD. Cortical aging differences and fracture implications for the human femoral neck. Bone. 1993;14(5):769–78. http://dx.doi.org/10.1016/8756-3282(93)90209-S. Medline:8268051

24. Martin RB, Burr DB, Sharkey NA. Mechanical properties of bone. In: Martin RB, Burr DB, Sharkey NA, editors. Skeletal tissue mechanics. New York: Springer; 1998. p. 127–80.

25. Cummings SR. How drugs decrease fracture risk: lessons from trials. J Musculoskelet Neuronal Interact. 2002;2(3):198–200. Medline:15758432

26. Seeman E. Bone quality: the material and structural basis of bone strength. J Bone Miner Metab. 2008;26(1):1–8. http://dx.doi.org/10.1007/s00774-007-0793-5. Medline:18095057

27. Jensen KS, Mosekilde L, Mosekilde L. A model of vertebral trabecular bone architecture and its mechanical properties. Bone. 1990;11(6):417–23. http://dx.doi.org/10.1016/8756-3282(90)90137-N. Medline:2078435

28. Silva MJ, Gibson LJ. Modeling the mechanical behavior of vertebral trabecular bone: effects of age-related changes in microstructure. Bone. 1997;21(2):191–9. http://dx.doi.org/10.1016/S8756-3282(97)00100-2. Medline:9267695

29. Bell GH, Dunbar O, Beck JS, et al. Variations in strength of vertebrae with age and their relation to osteoporosis. Calcif Tissue Res. 1967;1(1):75–86. http://dx.doi.org/10.1007/BF02008077. Medline:6060146

30. Mosekilde L, Mosekilde L, Danielsen CC. Biomechanical competence of vertebral trabecular bone in relation to ash density and age in normal individuals. Bone. 1987;8(2):79–85. http://dx.doi.org/10.1016/8756-3282(87)90074-3. Medline:3593611

31. Townsend PR, Rose RM, Radin EL. Buckling studies of single human trabeculae. J Biomech. 1975;8(3-4):199–201. http://dx.doi.org/10.1016/0021-9290(75)90025-1. Medline:1150688

32. Pugh JW, Rose RM, Radin EL. A structural model for the mechanical behavior of trabecular bone. J Biomech. 1973;6(6):657–70. http://dx.doi.org/10.1016/0021-9290(73)90022-5. Medline:4757484

33. Link TM, Md. Changes in trabecular bone structure assessed by high-resolution MRI in patients after transplantation. Adv Exp Med Biol. 2001;496:31–6. http://dx.doi.org/10.1007/978-1-4615-0651-5_4. Medline:11783623

34. Glüer CC, Wu CY, Jergas M, et al. Three quantitative ultrasound parameters reflect bone structure. Calcif Tissue Int. 1994;55(1):46–52. http://dx.doi.org/10.1007/BF00310168. Medline:7922789

35. Bouxsein ML, Radloff SE. Quantitative ultrasound of the calcaneus reflects the mechanical properties of calcaneal trabecular bone. J Bone Miner Res. 1997;12(5):839–46. http://dx.doi.org/10.1359/jbmr.1997.12.5.839. Medline:9144351

36. Ay A, Yurtkuran M. Influence of aquatic and weight-bearing exercises on quantitative ultrasound variables in postmenopausal women. Am J Phys Med Rehabil. 2005;84(1):52–61. http://dx.doi.org/10.1097/01.PHM.0000146500.85850.BE. Medline:15632489

37. Luria T, Matsliah Y, Adir Y, et al. Effects of a prolonged submersion on bone strength and metabolism in young healthy submariners. Calcif Tissue Int. 2010;86(1):8–13. http://dx.doi.org/10.1007/s00223-009-9308-9. Medline:19882096

38. Mazess R, Chesnut CH III, McClung M, et al. Enhanced precision with dual-energy X-ray absorptiometry. Calcif Tissue Int. 1992;51(1):14–7. http://dx.doi.org/10.1007/BF00296209. Medline:1393769

39. Kelly TL, Slovik DM, Schoenfeld DA, et al. Quantitative digital radiography versus dual photon absorptiometry of the lumbar spine. J Clin Endocrinol Metab. 1988;67(4):839–44. http://dx.doi.org/10.1210/jcem-67-4-839. Medline:3417851

40. Marshall D, Johnell O, Wedel H. Meta-analysis of how well measures of bone mineral density predict occurrence of osteoporotic fractures. BMJ. 1996;312(7041):1254–9. Medline:8634613

41. Siminoski K, Leslie WD, Frame H, et al.; Canadian Association of Radiologists. Recommendations for bone mineral density reporting in Canada. Can Assoc Radiol J. 2005;56(3):178–88. Medline:16144280

42. Jørgensen L, Jacobsen BK. Changes in muscle mass, fat mass, and bone mineral content in the legs after stroke: a 1 year prospective study. Bone. 2001;28(6):655–9. http://dx.doi.org/10.1016/S8756-3282(01)00434-3. Medline:11425655

43. Heaney RP. BMD: the problem. Osteoporos Int. 2005;16(9):1013–5. http://dx.doi.org/10.1007/s00198-005-1855-y. Medline:15776218

44. Beck TJ, Ruff CB, Warden KE, et al. Predicting femoral neck strength from bone mineral data. A structural approach. Invest Radiol. 1990;25(1):6–18. http://dx.doi.org/10.1097/00004424-199001000-00004. Medline:2298552

45. Faulkner KG, Cummings SR, Black D, et al. Simple measurement of femoral geometry predicts hip fracture: the study of osteoporotic fractures. J Bone Miner Res. 1993;8(10):1211–7. http://dx.doi.org/10.1002/jbmr.5650081008. Medline:8256658

46. Khoo BC, Wilson SG, Worth GK, et al. A comparative study between corresponding structural geometric variables using 2 commonly implemented hip structural analysis algorithms applied to dual-energy X-ray absorptiometry images. J Clin Densitom. 2009;12(4):461–7. http://dx.doi.org/10.1016/j.jocd.2009.08.004. Medline:19880052

47. Beck TJ, Oreskovic TL, Stone KL, et al. Structural adaptation to changing skeletal load in the progression toward hip fragility: the study of osteoporotic fractures. J Bone Miner Res. 2001;16(6):1108–19. http://dx.doi.org/10.1359/jbmr.2001.16.6.1108. Medline:11393788

48. El-Kaissi S, Pasco JA, Henry MJ, et al. Femoral neck geometry and hip fracture risk: the Geelong osteoporosis study. Osteoporos Int. 2005;16(10):1299–303. http://dx.doi.org/10.1007/s00198-005-1988-z. Medline:16082496

49. Bonnick SL. HSA: beyond BMD with DXA. Bone. 2007;41(1 Suppl 1):S9–12. http://dx.doi.org/10.1016/j.bone.2007.03.007. Medline:17459802

50. Webber CE, Papaioannou A, Winegard KJ, et al. A 6-mo home-based exercise program may slow vertebral height loss. J Clin Densitom. 2003;6(4):391–400. http://dx.doi.org/10.1385/JCD:6:4:391. Medline:14716053

51. Robling AG, Castillo AB, Turner CH. Biomechanical and molecular regulation of bone remodeling. Annu Rev Biomed Eng. 2006;8(1):455–98. http://dx.doi.org/10.1146/annurev.bioeng.8.061505.095721. Medline:16834564

52. Lang TF, Li J, Harris ST, et al. Assessment of vertebral bone mineral density using volumetric quantitative CT. J Comput Assist Tomogr. 1999;23(1):130–7. http://dx.doi.org/10.1097/00004728-199901000-00027. Medline:10050823

53. Mastmeyer A, Engelke K, Fuchs C, et al. A hierarchical 3D segmentation method and the definition of vertebral body coordinate systems for QCT of the lumbar spine. Med Image Anal. 2006;10(4):560–77. http://dx.doi.org/10.1016/j.media.2006.05.005. Medline:16828329

54. Habashy AH, Yan X, Brown JK, et al. Estimation of bone mineral density in children from diagnostic CT images: a comparison of methods with and without an internal calibration standard. Bone. 2011;48(5):1087–94. http://dx.doi.org/10.1016/j.bone.2010.12.012. Medline:21185418

55. Cointry GR, Capozza RF, Negri AL, et al. Biomechanical background for a noninvasive assessment of bone strength and muscle-bone interactions. J Musculoskelet Neuronal Interact. 2004;4(1):1–11. Medline:15615073

56. Wilhelm G, Felsenberg D, Bogusch G, et al. Biomechanical examinations for validation of the bone Strength-Strain Index, SSI, calculated by peripheral quantitative computed tomography. In: Lyrithis GP, editor. Musculoskeletal interactions. Vol. 2. Athens: Hylonome; 1999. p. 105–11.

57. Kontulainen SA, Johnston JD, Liu D, et al. Strength indices from pQCT imaging predict up to 85% of variance in bone failure properties at tibial epiphysis and diaphysis. J Musculoskelet Neuronal Interact. 2008;8(4):401–9. Medline:19147978

58. Nishiyama KK, Macdonald HM, Buie HR, et al. Postmenopausal women with osteopenia have higher cortical porosity and thinner cortices at the distal radius and tibia than women with normal aBMD: an in vivo HR-pQCT study. J Bone Miner Res. 2010;25(4):882–90. Medline:19839766

59. Cheng S, Sipilä S, Taaffe DR, et al. Change in bone mass distribution induced by hormone replacement therapy and high-impact physical exercise in post-menopausal women. Bone. 2002;31(1):126–35. http://dx.doi.org/10.1016/S8756-3282(02)00794-9. Medline:12110425

60. Ashe MC, Fehling P, Eng JJ, et al. Bone geometric response to chronic disuse following stroke: a pQCT study. J Musculoskelet Neuronal Interact. 2006;6(3):226–33. Medline:17142942

61. Pang MY, Ashe MC, Eng JJ. Muscle weakness, spasticity and disuse contribute to demineralization and geometric changes in the radius following chronic stroke. Osteoporos Int. 2007;18(9):1243–52. http://dx.doi.org/10.1007/s00198-007-0372-6. Medline:17401512

62. Pang MYC, Ashe MC, Eng JJ, et al. A 19-week exercise program for people with chronic stroke enhances bone geometry at the tibia: a peripheral quantitative computed tomography study. Osteoporos Int. 2006;17(11):1615–25. http://dx.doi.org/10.1007/s00198-006-0168-0. Medline:16896509

63. Ito M, Nakata T, Nishida A, et al. Age-related changes in bone density, geometry and biomechanical properties of the proximal femur: CT-based 3D hip structure analysis in normal postmenopausal women. Bone. 2011;48(3):627–30. http://dx.doi.org/10.1016/j.bone.2010.11.007. Medline:21087686

64. Crabtree N, Loveridge N, Parker M, et al. Intracapsular hip fracture and the region-specific loss of cortical bone: analysis by peripheral quantitative computed tomography. J Bone Miner Res. 2001;16(7):1318–28. http://dx.doi.org/10.1359/jbmr.2001.16.7.1318. Medline:11450708

65. MacIntyre NJ, Rombough R, Brouwer B. Relationships between calf muscle density and muscle strength, mobility and bone status in the stroke survivors with subacute and chronic lower limb hemiparesis. J Musculoskelet Neuronal Interact. 2010;10(4):249–55. Medline:21116061

66. Gordon CL, Lang TF, Augat P, et al. Image-based assessment of spinal trabecular bone structure from high-resolution CT images. Osteoporos Int. 1998;8(4):317–25. http://dx.doi.org/10.1007/s001980050070. Medline:10024901

67. MacIntyre NJ, Adachi JD, Webber CE. In vivo measurement of apparent trabecular bone structure of the radius in women with low bone density discriminates patients with recent wrist fracture from those without fracture. J Clin Densitom. 2003;6(1):35–43. http://dx.doi.org/10.1385/JCD:6:1:35. Medline:12665700

68. MacIntyre NJ, Adachi JD, Webber CE. In vivo detection of structural differences between dominant and nondominant radii using peripheral quantitative computed tomography. J Clin Densitom. 1999;2(4):413–22. http://dx.doi.org/10.1016/S1094-6950(06)60407-1. Medline:10677795

69. Riggs BL, Melton LJ III, Robb RA, et al. Population-based study of age and sex differences in bone volumetric density, size, geometry, and structure at different skeletal sites. J Bone Miner Res. 2004;19(12):1945–54. http://dx.doi.org/10.1359/jbmr.040916. Medline:15537436

70. Khosla S, Riggs BL, Atkinson EJ, et al. Effects of sex and age on bone microstructure at the ultradistal radius: a population-based noninvasive in vivo assessment. J Bone Miner Res. 2006;21(1):124–31. http://dx.doi.org/10.1359/JBMR.050916. Medline:16355281

71. Sornay-Rendu E, Cabrera-Bravo JL, Boutroy S, et al. Severity of vertebral fractures is associated with alterations of cortical architecture in postmenopausal women. J Bone Miner Res. 2009;24(4):737–43. http://dx.doi.org/10.1359/jbmr.081223. Medline:19113929

72. Nickolas TL, Stein E, Cohen A, et al. Bone mass and microarchitecture in CKD patients with fracture. J Am Soc Nephrol. 2010;21(8):1371–80. http://dx.doi.org/10.1681/ASN.2009121208. Medline:20395370

73. Kazakia GJ, Burghardt AJ, Link TM, et al. Variations in morphological and biomechanical indices at the distal radius in subjects with identical BMD. J Biomech. 2011;44(2):257–66. http://dx.doi.org/10.1016/j.jbiomech.2010.10.010. Medline:21071031

74. Laib A, Rüegsegger P. Comparison of structure extraction methods for in vivo trabecular bone measurements. Comput Med Imaging Graph. 1999;23(2):69–74. http://dx.doi.org/10.1016/S0895-6111(98)00071-8. Medline:10227372

75. Majumdar S. Magnetic resonance imaging of trabecular bone structure. Top Magn Reson Imaging. 2002;13(5):323–34. http://dx.doi.org/10.1097/00002142-200210000-00004. Medline:12464745

76. Krug R, Burghardt AJ, Majumdar S, et al. High-resolution imaging techniques for the assessment of osteoporosis. Radiol Clin North Am. 2010;48(3):601–21. http://dx.doi.org/10.1016/j.rcl.2010.02.015. Medline:20609895

77. Nikander R, Sievänen H, Heinonen A, et al. Load-specific differences in the structure of femoral neck and tibia between world-class moguls skiers and slalom skiers. Scand J Med Sci Sports. 2008;18(2):145–53. http://dx.doi.org/10.1111/j.1600-0838.2007.00643.x. Medline:18067528

78. Nikander R, Kannus P, Dastidar P, et al. Targeted exercises against hip fragility. Osteoporos Int. 2009;20(8):1321–8. http://dx.doi.org/10.1007/s00198-008-0785-x. Medline:19002370

79. Majumdar S, Newitt D, Mathur A, et al. Magnetic resonance imaging of trabecular bone structure in the distal radius: relationship with X-ray tomographic microscopy and biomechanics. Osteoporos Int. 1996;6(5):376–85. http://dx.doi.org/10.1007/BF01623011. Medline:8931032

80. Vieth V, Link TM, Lotter A, et al. Does the trabecular bone structure depicted by high-resolution MRI of the calcaneus reflect the true bone structure? Invest Radiol. 2001;36(4):210–7. http://dx.doi.org/10.1097/00004424-200104000-00003. Medline:11283418

81. Majumdar S, Genant HK, Grampp S, et al. Correlation of trabecular bone structure with age, bone mineral density, and osteoporotic status: in vivo studies in the distal radius using high resolution magnetic resonance imaging. J Bone Miner Res. 1997;12(1):111–8. http://dx.doi.org/10.1359/jbmr.1997.12.1.111. Medline:9240733

82. Majumdar S, Link TM, Augat P, et al, and the Magnetic Resonance Science Center and Osteoporosis and Arthritis Research Group. Trabecular bone architecture in the distal radius using magnetic resonance imaging in subjects with fractures of the proximal femur. Osteoporos Int. 1999;10(3):231–9. http://dx.doi.org/10.1007/s001980050221. Medline:10525716

83. Cao H, Ackerman JL, Hrovat MI, et al. Quantitative bone matrix density measurement by water- and fat-suppressed proton projection MRI (WASPI) with polymer calibration phantoms. Magn Reson Med. 2008;60(6):1433–43. http://dx.doi.org/10.1002/mrm.21771. Medline:19025909

84. Christiansen BA, Kopperdahl DL, Kiel DP, et al. Mechanical contributions of the cortical and trabecular compartments contribute to differences in age-related changes in vertebral body strength in men and women assessed by QCT-based finite element analysis. J Bone Miner Res. 2011;26(5):974–83. http://dx.doi.org/10.1002/jbmr.287. Medline:21542000

85. Keyak JH, Sigurdsson S, Karlsdottir G, et al. Male-female differences in the association between incident hip fracture and proximal femoral strength: a finite element analysis study. Bone. 2011;48(6):1239–45. http://dx.doi.org/10.1016/j.bone.2011.03.682. Medline:21419886

86. MacNeil JA, Boyd SK. Load distribution and the predictive power of morphological indices in the distal radius and tibia by high resolution peripheral quantitative computed tomography. Bone. 2007;41(1):129–37. http://dx.doi.org/10.1016/j.bone.2007.02.029. Medline:17442649

87. Wehrli FW, Ladinsky GA, Jones C, et al. In vivo magnetic resonance detects rapid remodeling changes in the topology of the trabecular bone network after menopause and the protective effect of estradiol. J Bone Miner Res. 2008;23(5):730–40. http://dx.doi.org/10.1359/jbmr.080108. Medline:18251704

88. Vilayphiou N, Boutroy S, Sornay-Rendu E, et al. Finite element analysis performed on radius and tibia HR-pQCT images and fragility fractures at all sites in postmenopausal women. Bone. 2010;46(4):1030–7. http://dx.doi.org/10.1016/j.bone.2009.12.015. Medline:20044044

89. MacNeil JA, Boyd SK. Bone strength at the distal radius can be estimated from high-resolution peripheral quantitative computed tomography and the finite element method. Bone. 2008;42(6):1203–13. http://dx.doi.org/10.1016/j.bone.2008.01.017. Medline:18358799

90. Wald MJ, Magland JF, Rajapakse CS, et al. Structural and mechanical parameters of trabecular bone estimated from in vivo high-resolution magnetic resonance images at 3 tesla field strength. J Magn Reson Imaging. 2010;31(5):1157–68. http://dx.doi.org/10.1002/jmri.22158. Medline:20432352

91. Bhagat Y, Magland JF, Rajapakse CS, et al. Micro-MRI based virtual bone biopsy detects structural remodelling effects upon anabolic drug treatment [Abstract]. J Bone Miner Res. 2010;25(Suppl 1):S468-9. http://dx.doi.org/10.1002/jbmr.5650251305